JACS
JOURNAL OF THE AMERICAN CHEMICAL SOCIETY
Communication
pubs.acs.org/JACS

Direct Imaging of Nanoscale Acidic Clusters in a Polymer Electrolyte Membrane

Sergey Yakovlev,[†] Xin Wang,[‡] Peter Ercius,[§] Nitash P. Balsara,[†,‡] and Kenneth H. Downing*[,∥]

[†]Materials Sciences Division, Lawrence Berkeley National Laboratory, Berkeley, California 94720, United States
[‡]Department of Chemical and Biomolecular Engineering, University of California, Berkeley, California 94720, United States
[§]National Center for Electron Microscopy, Lawrence Berkeley National Laboratory, Berkeley, California 94720, United States
[∥]Life Sciences Division, Lawrence Berkeley National Laboratory, Berkeley, California 94720, United States

Supporting Information

ABSTRACT: One of the factors hindering the development of technologies that rely on the use of proton-conducting polyelectrolyte membranes is the lack of control over the membrane morphology on the nanoscale. Of particular importance is the rearrangement and clustering of acidic groups, which may seriously degrade the electrical properties. Although electron microscopy is capable of imaging the morphology of the clusters, images of unmodified membranes with sufficient quality to discriminate between different proposed cluster morphology models have not been presented. Here we show the first determination of the cluster size distribution in a model polymer electrolyte membrane from electron micrographs of individual acidic clusters. Imaging of the sulfur-rich clusters by dark-field microscopy was facilitated by the spontaneous formation of thin, cluster-containing layers on the top and bottom surfaces of free-standing films with a thickness of ∼35 nm.

Polymer electrolyte membranes (PEMs) such as Nafion, comprising nanoscale hydrophilic and hydrophobic domains, are important for a variety of technologies such as purification of seawater,[1] hydrogen fuel cells,[2] and photoelectrochemical cells.[3] Ion transport in these systems is mediated by sulfonic acid groups present in the hydrophilic domains. While scattering experiments have revealed the presence of ionic clusters in both the dry and hydrated states, the sizes and shapes of the clusters remain controversial.[4−10] This controversy has impeded both the development of robust fundamental models for ion transport through the membranes and our ability to develop the next generation of membranes with superior transport properties. The purpose of this work is to resolve this controversy by direct imaging of the clusters and measuring the cluster size distribution.

X-ray scattering profiles of Nafion and other PEMs contain a broad peak with a characteristic length scale of ∼5 nm.[11] While it is generally assumed that this length scale represents the average distance between the clusters, the scattering data do not provide information about the sizes and shapes of the clusters. The problem lies in the fact that a single broad scattering peak cannot be used to determine the underlying structure uniquely. It is thus not surprising that a variety of different morphologies, such as connected spheres,[5] core−shell structures,[6] hard spheres,[7] bundles of rods,[8] parallel cylindrical channels,[10] and lamellar channels,[9] are all consistent with the scattering profiles obtained from Nafion. Electron microscopy can be used to distinguish between these morphologies, but micrographs obtained to date have not resolved this controversy. Previous electron microscopy (EM) studies[12−20] suffered from two limitations: (1) the electron micrographs were obtained from films with thicknesses much greater than the cluster size, and overlap of clusters in projection complicated the image interpretation;[21] (2) the contrast between the clusters and the background was always enhanced by either heavy-metal staining agents or replacing the protons by heavier cations using ion exchange. While the ion exchange procedure is a more controlled process than staining, the fact that ion exchange causes changes in the cluster morphology is well-established.[22] To date, electron micrographs of individual acidic clusters in PEMs have not been obtained.

In this work we show electron micrographs of individual ionic clusters in a PEM without the use of heavy-element stains or ion exchange. Our experiments were performed on a poly(styrene sulfonate)-*b*-poly(methylbutylene) (PSS−PMB) copolymer synthesized as described in ref 23. The molecular weights of the PSS and PMB blocks were 4.2 and 8.1 kg/mol, respectively, and the volume fraction of the PSS block was 0.27. The PSS block contained 40 mol % sulfonated monomers. Samples were prepared by dipping lacey carbon-coated EM grids into 1 wt % solutions of PSS−PMB in tetrahydrofuran (THF). The wet grids were dried slowly by placing them in a partially sealed vial above a small pool of THF at room temperature. Figure 1 shows typical top and cross-section views of an 80 nm thick sample obtained by bright-field electron tomography. Here we see alternating lamellae similar to those obtained from bulk samples of this copolymer as reported in ref 23. The dark PSS-rich domains have a smooth structure with relatively little granularity.

Annealing the samples in water vapor produced dramatic changes in morphology. The sample shown in Figure 1 was removed from the microscope, placed above a small pool of water in a partially sealed vial held at 50 °C for 50 h, and studied by high-angle annular dark-field (HAADF) scanning

Received: September 30, 2011
Published: November 22, 2011

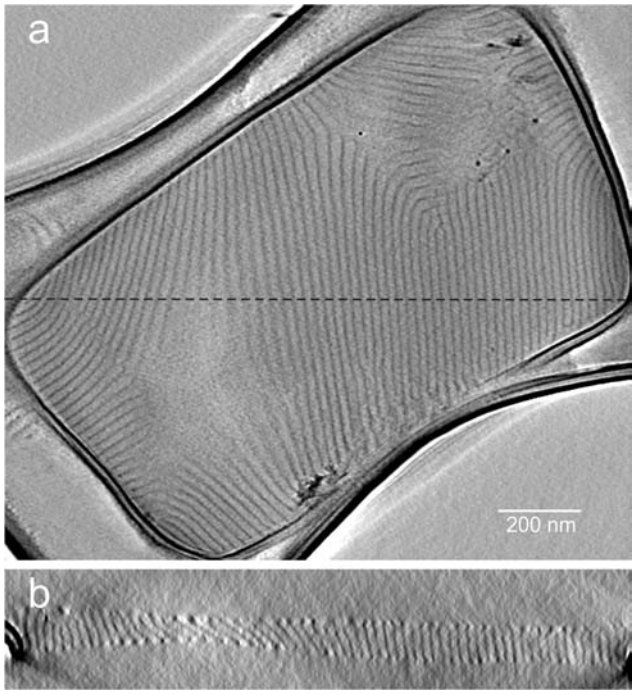

Figure 1. Slices of bright-field electron tomographic reconstruction of an 80 nm thick PSS–PMB film prepared by casting and annealing in THF vapor, showing the lamellar morphology: (a) top view; (b) cross-section view along the dashed line shown in (a).

transmission EM (STEM). The observed morphology resembles that of a honeycomb. This is most clearly seen in a HAADF image of an untilted film (Figure 2a). The size of the smallest cells in the honeycomb is ~20 nm, similar to the spacing of the lamellar morphologies seen in Figure 1. Careful examination of the honeycomb walls revealed that they consist of concentrated bright spots similar to the spots inside of the honeycomb. The brightness of these spots indicates that they consist of the heavier elements sulfur and oxygen, reflecting the locations of the sulfonic acid groups. The size, high contrast, and relatively small number of bright spots make it evident that they represent clusters rather than single sulfur atoms. It is logical to conclude that the honeycomb outlines reflect the sulfur-containing PSS-rich phase and that the nominally dark interior phase is the PMB-rich phase. This is consistent with the fact that PSS is the minor component, although the area fraction of the bright phase in Figure 2a is lower than the bulk volume fraction of PSS. While we show an image of a 35 nm thick sample in Figure 2a, samples with a variety of thicknesses were seen in different portions of the lacey carbon grid. The honeycomb morphology was seen in all cases (we could image films up to 500 nm thick) except films thinner than 25 nm. However, the clarity with which the morphology could be discerned decreased with increasing sample thickness.

Electron tomography was used to clarify the structure seen in Figure 2a. While the resolution of the 3D reconstruction is slightly lower than the resolution of the projection images because of the limited mechanical stability of the film which causes drift during image recording that affects the reconstruction, it is sufficient to reveal the structure of the film. Slices taken from the top, middle, and bottom parts of a 3D reconstruction of the film are shown in Figure 2b–d. The middle section (Figure 2c) shows the honeycomb morphology similar to that seen in Figure 2a, except for the absence of bright spots in the dark phase. The top and bottom sections are similar to each other, with numerous bright spots and only faint hints of the honeycomb structure. From this 3D view, the structure of the water-annealed membrane in Figure 2 is clear. Exposure to water at 50 °C results in the formation of PSS-rich

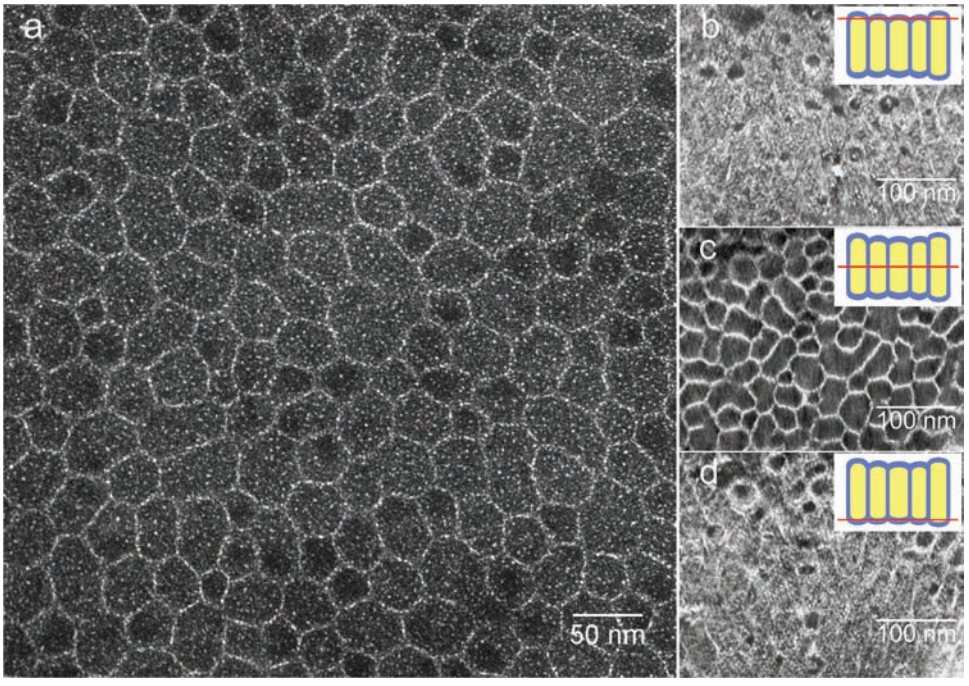

Figure 2. PSS–PMB film with a thickness of 35 nm prepared by casting and annealing in water vapor, showing the honeycomb morphology and ionic clusters (bright spots). (a) HAADF image obtained in projection. (b–d) Slices of HAADF tomographic reconstruction and (insets) diagrams indicating the positions of the slices in the cross section of the film: (b) top, (c) middle, and (d) bottom. The slices reveal that the ionic clusters are distributed uniformly near the top and bottom surfaces and are concentrated in the honeycomb wall structure.

layers on the top and bottom of the film. This arrangement shields the hydrophobic PMB-rich phase from the surrounding moist air. Such shielding on the surface of the block copolymer with a lower-interface-energy phase has been discussed previously.[24] The walls of the honeycomb are formed by the PSS-rich phase. These vertical lamellae are thinner than expected on the basis of the bulk volume fraction of PSS because a substantial fraction of the PSS chains in the sample covers the top and bottom surfaces. Both horizontal and vertical PSS-rich lamellae contain bright spots due to the presence of ionic clusters. The bright spots seen "inside" the honeycomb in Figure 2a are due to the projections of the spotted top and bottom surfaces (Figure 2b,d) rather than the presence of ionic clusters in the dark PMB-rich phase.

Placing the water-treated film back into a THF-containing vial for annealing resulted in a honeycomb-to-lamella transition. This is established in Figure 3, where we compare TEM

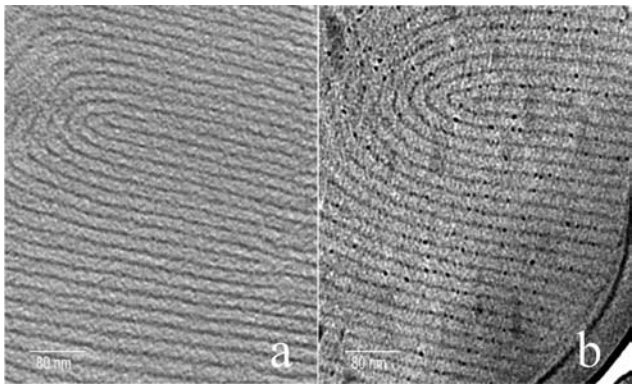

Figure 3. Slices from TEM tomographic reconstructions of thin PSS–PMB films prepared by (a) casting in THF vapor and (b) first casting in THF, then annealing in water vapor, and finally reannealing in THF. Both samples exhibit a lamellar morphology, but only sample (b) shows clearly distinguishable ionic clusters in the PSS phase.

tomographic reconstruction images right after casting (Figure 3a) and after first annealing in water and then in THF (Figure 3b). The major difference between the lamellae in Figure 3a,b is the presence of dark spots in the PSS-rich lamellae with sizes very similar to those seen in Figure 2. One may ask why the ionic clusters did not form when the sample was originally cast from THF (Figure 1). We propose that the equilibration of the glassy PSS phase is only possible when it is substantially plasticized by a good solvent such as water. It is known that THF is a poor solvent for PSS with a sulfonation level of 40%[25,26] as used in this work. At the same time THF is an excellent solvent for the PMB phase, which swells and reorganizes during the reannealing. As a side effect of reannealing, most of the thin films break, and only films with thicknesses greater than 100 nm survive. HAADF tomography of such thick samples produces lower-quality reconstructions than TEM bright-field tomography.

It was important to establish that the observed clusters were not a consequence of sample rearrangement due to electron beam damage.[27] We were only able to visualize the clusters using exposures of at least 10^3 e/nm^2. A series of images with increasing dose showed no change in the cluster morphology. The proof that the clusters we observed were not induced by irradiation below 10^3 e/nm^2 comes from the fact that none of the samples obtained from the initial THF casting without water vapor annealing showed evidence of clusters (e.g., Figure 1), irrespective of dose.

We used the image in Figure 2a to determine the size distribution of the ionic clusters. The areas within the honeycomb were ideally suited for determining the cluster size as a result of their minimal overlap. We used the integrated intensity of each cluster to determine the cluster size rather than directly measuring the diameter, since the images of individual clusters were noisy and pixilated. Clusters were sorted into classes according to integrated intensity, and the average of each class was used to determine the scaling between the diameter measured at half-maximum and the integrated intensity of the cluster. This scaling was used to determine the diameter of each cluster, and the diameter distribution thus obtained is shown in Figure 4 (see the Supporting Information

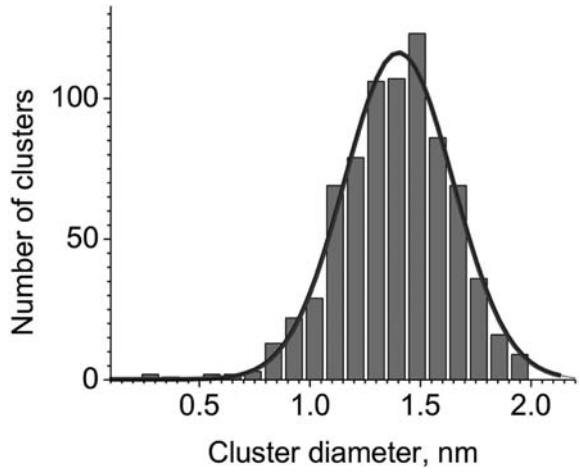

Figure 4. Histogram of ionic cluster size distribution (bars) and Gaussian fit (curve).

for more details). Fitting the experimental distribution to a Gaussian function, $f \sim \exp[-(d - d_{av})^2/2\sigma^2]$, we obtained the average cluster size, d_{av} = 1.4 nm, and the standard deviation, σ = 0.25 nm. The resulting fit is the smooth curve in Figure 4. The estimated uncertainty in d_{av} is ~14%. This fitting represents the first direct determination of the size distribution of acidic clusters in PEMs.

To conclude, we have succeeded in obtaining images of nanoscale ionic clusters in a PEM composed of alternating hydrophilic and hydrophobic lamellar domains. Exposing a 35 nm thick free-standing electrolyte film to moist air resulted in the formation of extremely thin cluster-containing layers at the electrolyte–air interfaces and a honeycomb morphology in the interior of the film. This morphology was ideally suited for direct imaging of ionic clusters by electron microscopy. The lamellar morphology with the clusters in the hydrophilic channels was recovered by re-exposing the film to THF-containing air. The shape and size distribution of the clusters reported here allows direct testing of theoretical models for structure formation and transport in PEMs. Since proton conductivity in PEMs is intimately linked to the nature of the ionic clusters,[28] the technique that we have developed will aid in future efforts to design and synthesize more effective PEMs. At this point, we have identified the nature of clusters in a particular PSS–PMB copolymer only. Further work is needed to determine the morphology of ionic clusters in other proton transporting membranes (e.g., Nafion).

■ ASSOCIATED CONTENT

Supporting Information

Description of EM methods and cluster size measurement details, including 3D graphs of the averaged intensity in each cluster class and a graph of the scaling between cluster intensity and diameter. This material is available free of charge via the Internet at http://pubs.acs.org.

■ AUTHOR INFORMATION

Corresponding Author

khdowning@lbl.gov

■ ACKNOWLEDGMENTS

We thank Drs. Robert M. Glaeser and John B. Kerr (LBNL) for helpful discussions. We also grateful to Dr. Puey Ounjai for the help with analysis of bright-field tomography data. Funding for this work was provided by the U.S. Department of Energy under Contract DE-AC02-05CH11231 through the Electron Microscopy of Soft Matter Program (electrolyte imaging) supported by the Office of Basic Energy Sciences, Materials Sciences and Engineering Division. Part of this work was performed at the National Center for Electron Microscopy and the Molecular Foundry at LBNL, which are supported by the Office of Science, Office of Basic Energy Sciences, U.S. Department of Energy under Contract DE-AC02-05CH11231.

■ REFERENCES

(1) Nagarale, R. K.; Gohil, G. S.; Shahi, V. K. *Adv. Colloid Interface Sci.* **2006**, *119*, 97.
(2) Smitha, B.; Sridhar, S.; Khan, A. A. *J. Membr. Sci.* **2005**, *259*, 10.
(3) Li, B.; Wang, L.; Kang, B.; Wang, P.; Qiu, Y. *Sol. Energy Mater. Sol. Cells* **2006**, *90*, 549.
(4) Mauritz, K. A.; Moore, R. B. *Chem. Rev.* **2004**, *104*, 4535.
(5) Hsu, W. Y.; Gierke, T. D. *J. Membr. Sci.* **1983**, *13*, 307.
(6) Fujimura, M.; Hashimoto, T.; Kawai, H. *Macromolecules* **1982**, *15*, 136.
(7) Yarusso, D. J.; Cooper, S. L. *Macromolecules* **1983**, *16*, 1871.
(8) Loppinet, B.; Gebel, G. *Langmuir* **1998**, *14*, 1977.
(9) Litt, M. *Polym. Prepr. (Am. Chem. Soc., Div. Polym. Chem.)* **1997**, *38*, 80.
(10) Schmidt-Rohr, K.; Chen, Q. *Nat. Mater.* **2008**, *7*, 75.
(11) Yarusso, D. J.; Cooper, S. L. *Polymer* **1985**, *26*, 371.
(12) Wang, W.; Chan, T.-T.; Perkowski, A. J.; Schlick, S.; Winey, K. I. *Polymer* **2009**, *50*, 1281.
(13) Ceynowa, J. *Polymer* **1978**, *19*, 73.
(14) Xue, T.; Trent, J. S.; Osseo-Asare, K. *J. Membr. Sci.* **1989**, *45*, 261.
(15) Li, C.; Register, R. A.; Cooper, S. L. *Polymer* **1989**, *30*, 1227.
(16) Dalmas, F.; Vonet, J.-F.; Randriamahefa, S.; Gaillet, C. *Macromol. Chem. Phys.* **2010**, *211*, 1765.
(17) Porat, Z.; Fryer, J. R.; Huxham, M.; Rubinstein, I. *J. Phys. Chem.* **1995**, *99*, 4667.
(18) Winey, K. I.; Laurer, J. H.; Kirkmeyer, B. P. *Macromolecules* **2000**, *33*, 507.
(19) Laurer, J. H.; Winey, K. I. *Macromolecules* **1998**, *31*, 9106.
(20) Seitz, M. E.; Chan, C. D.; Opper, K. L.; Baughman, T. W.; Wagener, K. B.; Winey, K. I. *J. Am. Chem. Soc.* **2010**, *132*, 8165.
(21) Handlin, D. L.; MacKnight, W. J.; Thomas, E. L. *Macromolecules* **1981**, *14*, 795.
(22) Eisenberg, A.; Navratil, M. *Macromolecules* **1974**, *7*, 90.
(23) Wang, X.; Yakovlev, S.; Beers, K. M.; Park, M. J.; Mullin, S. A.; Downing, K. H.; Balsara, N. P. *Macromolecules* **2010**, *43*, 5306.
(24) Kim, J.; Lee, J.; Lee, D. *Macromol. Res.* **2008**, *16*, 267.
(25) Carvalho, A. J. F.; Curvelo, A. A. S. *Macromolecules* **2003**, *36*, 5304.
(26) Gromadzki, D.; Černoch, P.; Janata, M.; Kůdela, V.; Nallet, F.; Diat, O.; Štěpánek, P. *Eur. Polym. J.* **2006**, *42*, 2486.
(27) Vesely, D. *Ultramicroscopy* **1984**, *14*, 279.
(28) Kim, S. Y.; Park, M. J.; Balsara, N. P.; Jackson, A. *Macromolecules* **2010**, *43*, 8128.